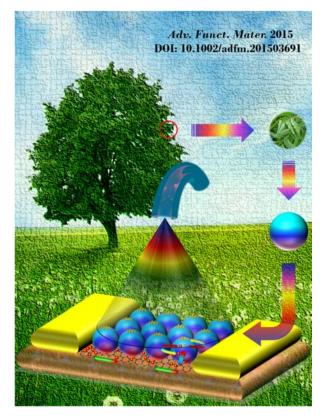# Electrical Polarization Induced Ultra-high Responsivity Photodetectors Based on Graphene and Graphene Quantum Dots

Hybrid quantum dot-graphene photodetectors have recently attracted substantial interest owing to their remarkable performance and low power consumption. However, the performance of the device greatly depends on the interfacial states and photogenerated screening field. As a consequence, the sensitivity is limited and the response time is relatively slow. In order to circumvent these challenges, we have designed a composite graphene and graphene quantum dot (GQD) photodetector on Lead Zirconate Titanate $(Pb(Zr_{0.2}Ti_{0.8})O_3)$ (PZT) substrates to form a ultra-sensitive photodetector over a wide range of illumination power. Under 325 nm UV light illumination, the device shows sensitivity as high as 4.06×10^9 AW^{-1}, which is 120 times higher than reported sensitivity of the same class of devices. Plant derived GQD has a broad range of absorptivity and is an excellent candidate for harvesting photons generating electron-hole pairs. Intrinsic electric field from PZT substrate separates photogenerated electron-hole pairs as well as provides the built-in electric field that causes the holes to transfer to the underlying graphene channel. The composite structure of graphene and GQD on PZT substrate therefore produces a simple, stable, and highly sensitive photodetector over a wide range of power with short response time, which shows a way to obtain high performance optoelectronic devices.

Adv. Funct. Mater. 2015
DOI: 10.1002/adfm.201503691

"This work has been identified as very important and very urgent by all of the reviewers as well as the editor of the journal and has been published with maximum priority."

FULL PAPER

Electrical-Polarization-Induced Ultrahigh Responsivity Photodetectors Based on Graphene and Graphene Quantum Dots

Golam Haider, Prathik Roy, Chia-Wei Chiang, Wei-Chun Tan, Yi-Rou Liou, Huan-Tsung Chang, Chi-Te Liang, Wei-Heng Shih,* and Yang-Fang Chen*

Hybrid quantum dot–graphene photodetectors have recently attracted substantial interest because of their remarkable performance and low power consumption. However, the performance of the device greatly depends on the interfacial states and photogenerated screening field. As a consequence, the sensitivity is limited and the response time is relatively slow. In order to circumvent these challenges, herein, a composite graphene and graphene quantum dot (GQD) photodetector on lead zirconate titanate $(Pb(Zr_{0.2}Ti_{0.8})O_3)$ (PZT) substrates has been designed to form an ultrasensitive photodetector over a wide range of illumination power. Under 325 nm UV light illumination, the device shows sensitivity as high as 4.06×10^9 A W^{-1}, which is 120 times higher than reported sensitivity of the same class of devices. Plant derived GQD has a broad range of absorptivity and is an excellent candidate for harvesting photons generating electron–hole pairs. Intrinsic electric field from PZT substrate separates photogenerated electron–hole pairs as well as provides the built-in electric field that causes the holes to transfer to the underlying graphene channel. The composite structure of graphene and GQD on PZT substrate therefore produces a simple, stable, and highly sensitive photodetector over a wide range of power with short response time, which shows a way to obtain high-performance optoelectronic devices.

1. Introduction

Graphene is light, strong, nontoxic, and stable having a high carrier mobility as well as high optical transparency, making it a good material for optoelectronic devices.[1–6] Because single layer graphene (SLG) does not have optical bandgap,[4,7] it can harvest only 2.3% of optical photons.[8] On the other hand, graphene has low density of states around Dirac point which makes its conductivity sensitive to perturbation from connected materials.[7,9] Hence, composites of graphene and a photon absorbing material is an effective way to create sensitive optoelectronic devices.[10–14] On the other hand, with the same allotrope of carbon having the dimension down to its Bohr radius, graphene quantum dot (GQD) is of great interest due to its size tunable optical response with large optical absorbance and the capability to generate multiple carriers.[15–17] In addition, the combination of SLG and GQD have a unique band

G. Haider
Department of Engineering and System Science
National Tsing Hua University
Hsinchu 300, Taiwan, R. O. China
G. Haider
Nano-Science and Technology Program
Taiwan International Graduate Program
Academia Sinica
Taipei 115, Taiwan, R. O. China
G. Haider
National Tsing Hua University
Hsinchu 300, Taiwan, R. O. China
G. Haider, C.-W. Chiang, W.-C. Tan, Y.-R. Liou,
Dr. C.-T. Liang, Prof. Y.-F. Chen
Department of Physics
National Taiwan University
No. 1, Sec. 4, Roosevelt Road
Taipei 106, Taiwan, R. O. China
E-mail: yfchen@phys.ntu.edu.tw

G. Haider, C.-W. Chiang, W.-C. Tan, Y.-R. Liou,
Dr. C.-T. Liang, Prof. Y.-F. Chen
Center for Emerging Material and Advanced Devices
National Taiwan University
No. 1, Sec. 4, Roosevelt Road
Taipei 106, Taiwan, R. O. China
Dr. P. Roy, Prof. H.-T. Chang
Department of Chemistry
National Taiwan University
No. 1, Sec. 4, Roosevelt Road
Taipei 106, Taiwan, R. O. China
Dr. C.-T. Liang
Geballe Laboratory for Advanced Materials
Stanford University
Stanford, CA 94305, USA
Prof. W.-H. Shih
Department of Materials Science and Engineering
Drexel University
Philadelphia, PA 19104, USA
E-mail: shihwh@drexel.edu

alignment which favors selective transfer of photogenerated carriers from GQD to graphene. The GQD has been reported to have consistent photoresponse under continuous excitation with Xe lamp (450 W cm^{-2}) for 1000 h.[17]

Piezoelectric materials have been extensively used in electro-mechanical applications as a converter of ambient mechanical energy to electricity.[18–20] Recent illustrations of using piezo-electric substrate to tune transport mechanism in microelec-tronic devices have drawn significant attention to optoelectronic device applications.[21,22] During the past few years, we devel-oped optothermal field effect transistor by replacing the gate dielectric SiO$_2$ by lead zirconate titanate (PZT).[23] Chemical vapor deposition (CVD) grown graphene has been transferred to PZT substrate and covered by poly(3-hexylthiophene-2,5-diyl) (P3HT) to make hybrid graphene–organic photodetectors.[24] The intrinsic electric field of PZT substrate can pass through SLG and is shown to help the transfer of photogenerated holes of P3HT to the graphene channel, enhancing the responsivity ten times that of SiO$_2$ substrate.[24]

Indeed, graphene based composites have enormous poten-tial of becoming highly sensitive photodetectors due to their ultrahigh response to the incoming photons taking advan-tage of high carrier mobility of graphene and high absorption property of the composite material.[25–29] However, at lower illumination power, the defect trap states at the graphene/photoabsorber interface limit the photoresponsivity (R_{Ph}) to ≈10^{7}A W^{-1}. Meanwhile, the device suffers an abrupt fall of R_{Ph} at higher illumination power because of the screening of the built-in electric field by the accumulation of charges in the photon absorbing materials.[10] Here, we create a com-posite photodetector of graphene and GQD on PZT substrate showing enhanced R_{Ph} in a wide range of illumination power

with rapid response time, taking advantage of the electric field provided by the piezoelectric substrate. Since PZT, gra-phene, and GQD are stable in atmosphere, the composite photodetector will have a wide range of applications in optical communication, remote sensing, optoelectronic circuits, bio-medical imaging, and quantum information technology.

2. Results and Discussion

2.1. Device Structures and Characteristics of Component Materials

To demonstrate the effect of PZT substrates, two different devices have been designed on PZT substrates having oppo-site polarization of PZT electric field (E_P), which is parallel and antiparallel to the direction of built-in electric field (E_B). A standard device is also built on SiO$_2$ for comparison. More detailed description of device fabrication is given in the Experi-mental Section. The structure of the composite photodetector is shown in **Figure 1**a with GQD particles on top of graphene that was deposited on the PZT substrate having polarization in the vertical direction, i.e., parallel to E_B. The device on PZT having E_P pointing downward, termed DPZT is shown in Figure 1b. The device with E_P pointing upward is termed UPZT. The energy band diagram with different electric fields present in the composite is shown in Figure 1c for the DPZT device under the illumination of 325 nm laser. Transmission electron microscope (TEM) image of GQD coated on the device as a photon har-vester is shown in **Figure 2**a indicating individual particles with average size of 5–7 nm. The appearance of D band and G band around 1300 and 1544 cm^{-1}, respectively, in Raman spectra
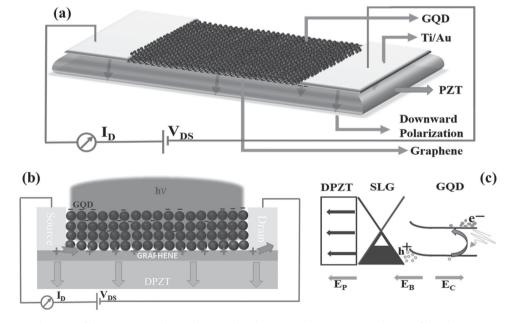

Figure 1. a) Schematic diagram of device on PZT having downward polarization. b) Cross-sectional view of the device. c) Energy band diagram with different directions of electric field originated after coating the GQDs and illuminated by laser. E_B is the built-in electric field at graphene–GQD junction, directed from GQD to graphene. E_P represents the electric field due to the bound charges in the PZT substrate directed parallel to E_B. E_C is the electric field due to the parallel plate capacitor effect when electrons are accumulated in GQD and holes being transferred to graphene, as in (b). E_C is directed opposite to E_B.
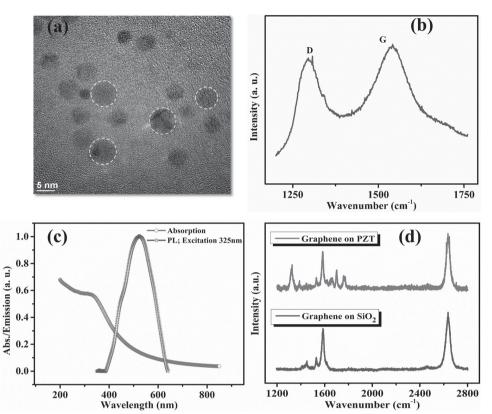
Figure 2. a) High-resolution transmission electron microscope (HRTEM) image of graphene quantum dot (GQD). b) Raman spectrum of GQD at 488 nm excitation. c) UV–vis absorption (red) and photoluminescence emission (blue) of GQD at 325 nm excitation. d) Raman spectrum of single layer graphene (SLG) on PZT (red) and SiO$_2$ (blue) at 633 nm excitation.

in Figure 2b confirms the GQDs are composed of graphene flakes. The intensity ratio of D to G band is found to be around 0.90 corresponding to a GQD of 1–3 layers of graphene.[17,30,31] Figure 2c indicates UV–vis absorption and normalized photoluminescence (PL) emission of GQD. The absorption spectrum shows that GQDs have strong absorbance starting around 600 nm. The PL emission spectrum shows the emission peak located around 523 nm under the illumination of He—Cd laser beam of wavelength 325 nm. Raman spectrum of the graphene layer on PZT and SiO$_2$, respectively, is shown in Figure 2d. The absence of D band of the graphene on SiO$_2$ confirms that the graphene is almost defect free.[32,33] The appearance of D band around 1323 cm^{-1} with the sample on PZT is likely due to PZT's rough surface. The small spikes around the G peak are the Raman signals from the PZT substrate. The intensity ratio of G to 2D band is 0.72 (<1) confirming that it is single layer graphene.[34]

2.2. Responsivity of Device Performance

The device performance has been examined by measuring the I_D value as a function of V_{DS} as shown in **Figure 3**. The change of conductance in graphene channel after the illumination of UV-laser of various power is described by the photoresponsivity of the device as Equation (1), where ΔI is the change in photocurrent ($\Delta I = |I_{Illumination} - I_{Dark}|$) and P

is the total UV-laser illumination power on the device active area (6 μm × 19 μm)[11,12]

$$R_{Ph} = \frac{\Delta I(A)}{P(W)}. \tag{1}$$

Figure 3a shows the I_D versus V_{DS} plot taken at illumination power varying from 25 to 525 fW for DPZT devices. A clear change in photocurrent from dark to light has been observed at different light intensity down to several fW laser power. A highest R_{Ph} of 4.06×10^9 A W^{-1} was obtained. Figure 3b represents the I_D–V_{DS} plot for the device on SiO$_2$. The data have been taken with illumination power varying from 0.3 to 900 pW. There is relatively smaller change in current resulting in a maximum photoresponsivity of ≈3 × 10^7 A W^{-1}, which is in good agreement with previous results from Cheng et al.[12] and Konstantatos et al.[10] The I_D–V_{DS} curve for the device on UPZT is shown in Figure 3c. Very little current change was found for the power down to several pW. The device shows maximum photoresponsivity of 1.5×10^5 A W^{-1}. A comparison of photoresponsivity for the three different devices under a wide power range is plotted in Figure 3d. At lower power, the DPZT device shows a transpicuous enhancement of responsivity by 120 times than SiO$_2$ device. In addition, the responsivity for DPZT device is >10^7 up to nW range of power, while for SiO$_2$ device it starts to drop abruptly at a power higher than ≈50 fW. On the other hand, the opposite effect of the polarization in UPZT device has reduced the responsivity ≈200 times than SiO$_2$
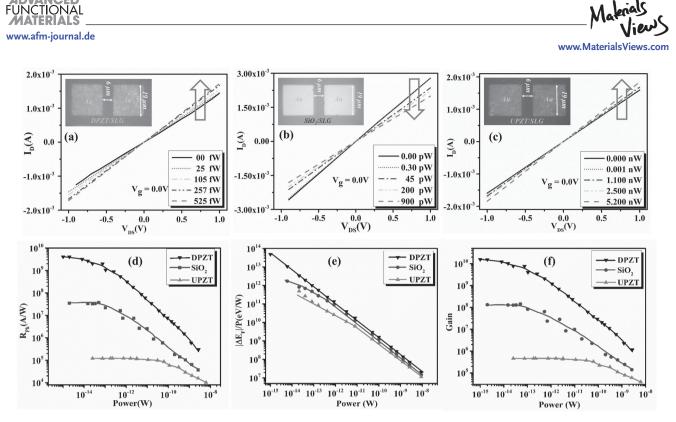
Figure 3. a–c) The dependence of I_D on V_{DS} for different laser power, of the devices deposited on DPZT, SiO$_2$, and UPZT substrate, respectively. Insets in the pictures are the optical microscopy images of the respective devices. Note that DPZT device can provide a significant photocurrent at an illumination power ≈fW, whereas SiO$_2$ and UPZT device need >100 fW and >pW, respectively. No gate voltage is applied for the measurement. d) Dependence of photoresponsivity (R_{Ph}) of the devices on applied power for three different substrates. R_{Ph} was calculated by Equation (1) at V_{DS} = 1.0 V. e) Shift of Fermi energy per unit change of input power for the devices as a function of incoming photon power. f) Photocurrent gain (Γ) of the three devices. All the lines in (d)–(f) are drawn to guide the eye.

device. We performed the photocurrent measurement of SLG/DPZT, SLG/SiO$_2$, and SLG/UPZT as shown in Figure S1 (Supporting Information). The small and similar changes of photocurrent related to the gas molecular desorption[35] confirm that the optical bandgap excitation of ferroelectric substrate PZT has no contribution in the measured photocurrent, because the photon energy of the incident light is smaller than the bandgap of PZT.[36]

2.3. Underlying Mechanism for Ultrahigh Responsivity

To explain the reason behind the high photoresponsivity, we have investigated the change in Fermi energy (ΔE_F) with laser power by performing transport measurement over a wider range of laser power. We measured the magnitude of Dirac point shift, $|\Delta V_g|$ as a function of total illumination power (P) on the device and calculated Fermi energy change by using Equation (2)

$$\Delta E_F = \text{Sign}\left(\Delta V_g\right)\hbar v_F\left(\alpha\pi\left|\Delta V_g\right|\right)^{1/2}, \qquad (2)$$

where α is gate capacitance and v_F is the velocity of the carriers at Fermi level.[37] A plot of $|\Delta V_g|$ and $|\Delta E_F|$ against laser power (P) is shown in Figures S2 and S3 (Supporting Information). Figure 3e shows the variation of E_F per unit power, $|\Delta E_F|/P$, against the applied power (P) for the three devices. A linear change in $|\Delta E_F|/P$ with applied power (P) for DPZT signifies a

smooth change in E_F of graphene with P, over the whole laser power range. A change in slope of $|\Delta E_F|/P$ versus P curve for SiO$_2$ and UPZT in lower power range indicates a much smaller change in E_F with power for the two devices. Thus, a loss of photogenerated carriers occurred during charge carrier transfer to the graphene for these two devices which can be correlated to carrier trapping in the graphene–GQD interface defect states. This could be the reason of the limited responsivity ≈10^7 for SiO$_2$ and ≈10^5 for UPZT device.

More clear description can be given by accounting different electric fields present in the composites. As the E_F of graphene is very sensitive to external perturbations, different electric field inside the composite has different contribution to the E_F as the laser power is varied. For graphene–GQD system there is a built-in electric field (E_B) at the graphene–GQD interface. After the generation of e–h pairs by the illumination of photons, holes/electrons are transferred to the graphene keeping electrons/holes on the GQD. An additional electric field, (E_C), directed opposite to the built-in electric field, is generated due to the charge accumulation.[10] The effective field experienced by the carriers can be described as $E_{eff} = E_B - E_C$. At higher illumination power more electron–hole pairs are generated. Hence, more electrons/holes are accumulated on GQD, which makes E_C larger. At the same time, more holes/electrons are transferred to the graphene which makes Fermi level lower/higher reducing E_B. Thus, E_{eff} decreases very rapidly with increasing laser power (until the net e–h pair generation becomes saturated in the light absorber), which results

www.MaterialsViews.com

ADVANCED
FUNCTIONAL
MATERIALS
www.afm-journal.de

FULL PAPER

in a rapid reduction of photoresponsivity at power >50 fW for the device on SiO$_2$. In contrast, for the device on DPZT, the intrinsic electric field of the PZT substrate (E_P) has the same direction as E_B, as shown in Figure 1c. The effective electric field (E_{eff}) to the carriers can be expressed as $E_{eff} = E_B + E_P - E_C$. Thus, E_P provides an extra drift force to the photogenerated carriers resulting in lesser recombination at the interfacial trapping states. Hence, we have observed a linear change in $|\Delta E_F|/P$, i.e., a linear change of graphene Fermi energy with power making the device ultrasensitive at lower laser power. Furthermore, the presence of E_P counter balances the effect of E_C, which maintains the responsivity >10^7 A W^{-1} up to laser power ≈nW. On the other hand, the opposite direction of E_P with E_B for UPZT device results in $E_{eff} = E_B - (E_P + E_C)$, causing rapid reduction of responsivity as well as less photocurrent gain.

It is worth mentioning that the photoresponsivity can be further enhanced by reducing the device dimension. Reducing the channel length, the flow path of holes on graphene causes more recirculation of holes on graphene channel and enhances the responsivity. Furthermore, reducing the channel length can increase the in-plane electric field applied by V_{DS}, which is desirable for low power devices.

2.4. Photocurrent Gain of Device Performance

Another way of comparing the effect of polarized field on the device is to look at the dimensionless photocurrent gain as defined in the following Equation (3)

$$\Gamma = \frac{\Delta I/q}{P/h\nu} \times \frac{1}{\eta},$$ (3)

where Γ is the photocurrent gain, ΔI is the current difference between illumination and dark condition, q is the electronic charge, P is the incident power, $h\nu$ is the photon energy of incident light, and η is the quantum efficiency for carrier generation per unit photon absorption.[38] For simplicity in comparing the effect of substrate, η is assumed to be 1.[11] The calculated gain is plotted in Figure 3f. It shows that the maximum photocurrent gain are ≈10^{10}, 10^8, and 10^5 for GQD/graphene/DPZT, GQD/graphene/SiO$_2$, and GQD/graphene/UPZT, respectively. The results are consistent with that found in Figure 3d.

2.5. Substrate Dependent Charge Carrier Transport in the Composite Device

To investigate the carrier transport properties in the device, we have analyzed the transport characteristics in different conditions such as (i) graphene on PZT/SiO$_2$ without GQD, (ii) graphene on PZT/SiO$_2$ with GQD in the dark, and (iii) graphene on PZT/SiO$_2$ with GQD under light illumination at similar power. **Figure 4**a–c shows the transfer characteristics of the DPZT, SiO$_2$, and UPZT devices in different situations as described in the figures. It is observed that after spin-coating the GQD on DPZT device, ΔV_g is 41.50 V toward left (i.e., $\Delta V_g = -41.5$ V), while for SiO$_2$, it is 18.95 V toward right (i.e., $\Delta V_g = +18.95$ V). Furthermore, under 325 UV-light illumination, ΔV_g is 24.42 V toward right ($\Delta V_g = +24.42$ V) for DPZT, whereas it is 15.80 V to
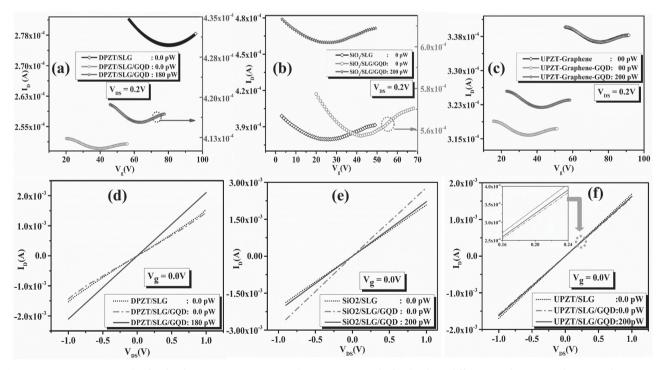

Figure 4. a–c) I_D versus V_g plot for the device on DPZT, SiO$_2$, and UPZT, respectively, for the three different conditions: graphene, graphene–GQD, and graphene–GQD under light illumination, with V_{DS} maintained at 0.2 V. Note that the scale of the right axis is significantly higher than that of the left axis indicating much higher current. d–f) I_D versus V_{DS} curves taken at the same conditions keeping V_g at 0 V. 325 nm laser was used to illuminate the device.

FULL PAPER

the left for SiO$_2$ ($\Delta V_g = -15.80$ V). (UPZT device behaves the same as the DPZT device with smaller ΔV_g.) A change in Fermi level (ΔE_F) has been estimated using the shift of Dirac point (ΔV_g) by Equation (2), as shown in Table S1 (Supporting Information).

Drain current (I_D) as a function of drain to source voltage (V_{DS}) was measured, in the same conditions as above, and the results are shown in Figure 4d–f for the DPZT, SiO$_2$, and UPZT devices, respectively. Figure 4d shows a decrease in conductance once GQD is coated on the device. This is due to the fact that electrons from GQD are transferred to graphene, which makes the graphene layer less p-type. Under light illumination, the photogenerated holes from GQD are transferred to the graphene layer due to favorable band alignment making graphene more p-type and causing an increase of conductance. On the other hand, after coating the GQD on the SiO$_2$ device the conductance increases due to the transfer of electrons from graphene to GQD which makes the graphene channel more p-type. After illumination of light the conductance decreases because of photogenerated electron transferred from GQD to graphene which explains the I_D–V_{DS} characteristics in Figure 4e. In Figure 4f, UPZT shows similar behavior as DPZT with smaller magnitudes.

The optoelectronic phenomena can be understood by the band diagrams of the various devices shown in **Figure 5**. SiO$_2$ wafer is a well-established material with good quality and little

defects on its smooth surface. On the other hand, PZT is a multicomponent material having many defects on its surface. After depositing graphene on substrates, the electrons from graphene may transfer to the interface defect states of both SiO$_2$ and PZT. As PZT having more defects at the interface, more electrons will be transferred to PZT than SiO$_2$. Thus, we expect ΔV_g to be larger for the PZT device than the SiO$_2$ device, consistent with the measurement results. Therefore, the Fermi level of graphene on PZT device will be shifted downward more than that on SiO$_2$, as shown in Figure 5a,d,g.

The GQD is a p-type material[27,31,39] and its E_F is closer to the E_F of freestanding SLG. Due to the different shift of E_F by different substrate, the E_F of graphene/PZT will have a lower value while the E_F of graphene/SiO$_2$ will have a higher value than that of GQD. Thus, after spin-coating the GQD on graphene/PZT, the electrons from GQD will move to SLG which creates a built-in electric field in the interface directed from GQD to graphene and band bending to the upward direction toward graphene as shown in Figure 5b,h. On the other hand, after spin-coating the GQD on graphene/SiO$_2$, electrons from SLG will move to GQD generating a built-in electric field to the opposite direction and downward band bending toward graphene as shown in Figure 5e. Thus, the transfer characteristics of DPZT devices show left shift of ΔV_g (positive ΔV_g) whereas SiO$_2$ shows right shift of ΔV_g (negative ΔV_g), causing the Fermi level of graphene to increase for PZT devices and
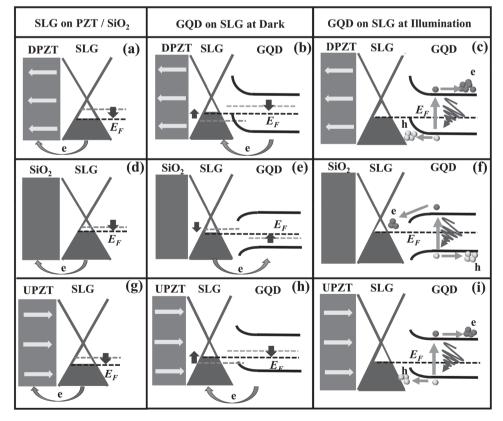

Figure 5. Energy band diagram of the devices at different conditions: a,d,g) Change in Fermi level (E_F) after transferring single layer graphene (SLG) on DPZT, SiO$_2$, and UPZT, respectively. b,e,h) The energy band diagram after spin-coating the GQD on the top of SLG/DPZT, SLG/SiO$_2$, and SLG/UPZT, respectively. c,f,i) Transport of photogenerated carriers after the illumination of 325 UV laser on the device. The charges flow in different direction depending upon the nature of band bending. The effects of UPZT are similar to that of DPZT except at smaller magnitude and smaller band bending.
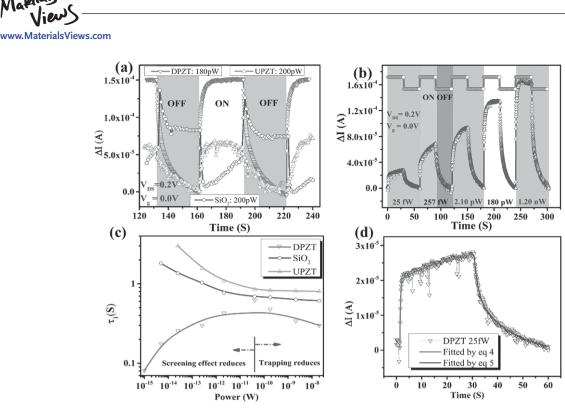
www.MaterialsViews.com

ADVANCED
FUNCTIONAL
MATERIALS
www.afm-journal.de

FULL PAPER

Figure 6. a) Transient response of the devices designed on DPZT, SiO$_2$, and UPZT for 180, 200, and 200 pW, respectively, at 325 nm illumination. b) Temporal photocurrent response of DPZT device on different power of incoming 325 nm laser. Red curve indicates the transient behavior of incoming laser while blue line is the response of DPZT device on incoming radiation. c) Dependence of response time of three different devices on incoming power. Response time (τ_1) was calculated by Equation (4). d) Curve showing the fitting of transient response curve with Equations (4) and (5).

decrease for SiO$_2$ devices, respectively. Under the illumination of UV-laser, due to the nature of built-in electric field, photogenerated holes transfer to graphene, which reduces the E_F for graphene/PZT device (Figure 5c,h), but photogenerated electrons transfer to graphene/SiO$_2$ (Figure 5f) which increases its E_F. These behaviors are consistent with the results of Dirac point shift measurement. Due to the nature of built-in electric field, graphene/SiO$_2$ devices have negative photocurrent, while graphene/PZT devices have positive photocurrent.

According to our observation, the relative position of Fermi energy of graphene and GQD determines the nature of built-in electric field which causes the transfer of photogenerated charges from GQD to graphene, which in turn sets the polarity of a photodetector. In a real device, if the Fermi energy of graphene (E_{FG}) − Fermi energy of QD (E_{FQD}) > 0, the composite device works as a negative polarity photodetector, whereas $E_{FG} − E_{FQD} < 0$ produces a positive polarity photodetector.

2.6. Dynamic Photoresponse and Response Time

A comparison of dynamic response curve with different substrates is shown in **Figure 6**a. For simplicity, we compared the change in photocurrent ($\Delta I = I_{\text{Illumination}} − I_{\text{Dark}}$) rather than the photocurrent itself. It is clear from the figure that ΔI for GQD/graphene/DPZT is higher than GQD/graphene/SiO$_2$, which is in turn higher than that of GQD/graphene/UPZT. The result is obvious due to the bound charge effect of PZT substrate which gives intrinsic electric field in and out of favor of charge transfer for GQD/graphene/DPZT and GQD/graphene/UPZT,

respectively. A comparison of dynamic behavior of the GQD/graphene/DPZT device under different illumination power is also shown in Figure 6b. The transient behavior of the devices can be fitted with Equations (4) and (5) as shown below for switch on and switch off state, respectively[25,40]

$$\Delta I_{DS} = \Delta I_1 \left\{ 1 − \exp\left(−t / \tau_1\right) \right\} + \Delta I_2 \left\{ 1 − \exp\left(−t / \tau_2\right) \right\} \quad (4)$$

$$\Delta I_{DS} = \Delta I_3 \left\{ \exp\left(−t/\tau_3\right) \right\} + \Delta I_4 \left\{ \exp\left(−t/\tau_4\right) \right\}. \quad (5)$$

Here, τ_1 and τ_2 can be correlated with relaxation time to transfer holes from GQD to graphene and charge transfer inside GQD matrix. In Equation (5), τ_3 and τ_4 can be correlated as the lifetime of electrons and charge transfer inside GQD network (similar to τ_2), respectively. Transient response fitted by Equations (4) and (5) is shown in Figure 6d. Extracted value of all time constants are tabulated in **Table 1**. Lower values of τ_1 and τ_2 for DPZT and higher values for UPZT device compared

Table 1. Relaxation time extracted by using Equations (3) and (4) at an incident power of 20 nW.

Relaxation time [s]	DPZT	SiO$_2$	UPZT
τ_1	0.301	0.612	0.801
τ_2	1.161	5.041	10.202
τ_3	4.930	0.951	0.720
τ_4	15.27	12.313	8.520

FULL PAPER

to SiO_2 indicate that E_P has strong effect on charge transfer. Presence of E_P in DPZT provides an additional field with built-in electric field which helps transfer the charges faster than that in SiO_2. Data shown in Table 1 are taken under the illumination of 20 nW power. A minimum value of 81 and 502 ms of τ_1 and τ_2, respectively, for DPZT is found at 1 fW power, which is ten times faster than that of the SiO_2 device. A comparison of the value of τ_1 for a wide range of power is shown in Figure 6c. The enhancement of τ_1 at lower power for UPZT and SiO_2 can be correlated to the carrier trapping at the graphene–GQD interface. The anomalous nature of τ_1 for DPZT can be inferred as combined effects of carrier trapping and screening of E_B by E_C. When the illumination power is reduced from higher to lower, τ_1 increases, which is due to small carrier trapping effect similar to the standard SiO_2 device. At even lower power (<50 pW) the device responds faster, which could be due to less screening in E_B. The behavior of dynamic response curve in Figure 6b changes with power is consistent with the earlier responsivity and response time results.

3. Conclusions

In laser based fiber-optic communication system, a highly sensitive photodetector is desired to decode the incoming optical signals to electrical signal. A photodetector with ultrahigh responsivity in a wide range of illumination power is thus necessary to design the decoders. In principle, the special separation of photogenerated charges and ability of its transfer to the underlying graphene channel plays a dominating role over the control of responsivity and response time. Thus, trapping of the photogenerated carriers at the interface limits the responsivity. Charging effect in GQD under intense illumination drastically reduces the responsivity of the device due to the screening of built-in electric field. Here, we provide a feasible approach to overcome the trapping as well as screening effects in the device to maintain the high responsivity over a wide range of illumination power with the assistance of PZT substrates. The photodetector on PZT substrate with polarization toward built-in electric field has an ultrahigh responsivity exceeding 10^9 A W^{-1} and ≈10 times faster response. The device is simple to fabricate and stable in normal atmosphere. In addition, the GQD is derived from Neem (*Azadirachta indica*) leaf which also shows a pathway for plant-inspired optoelectronics.

4. Experimental Section

Commercial, 127 µm thick, PZT (T105-A4E-602, Piezo-System, Boston, MA) was used as a substrate. It was electroded by Ni and poled perpendicular to its surface by the manufacturer. The electrodes were removed by HNO_3 etching and used as a substrate for graphene deposition.

GQD was prepared according to a previous report.[17] In the method, 250 mg of Neem leaf was extracted in 20 mL of DI water. The mixture was hydrothermally treated at 300 °C for 8 h in an autoclave. To remove the larger flakes, it was then centrifuged at centrifuging force of 25 000 for 20 min. The GQD solution was then dialyzed in ultrapure water for 24 h. The solution was then dried at 60 °C in an oven for overnight to get pure GQD. The photoluminescence, Raman, and UV–vis absorption spectrum was taken at ambient condition. 325 and 488 nm laser was used to study photoluminescence and Raman spectrum, respectively.

Graphene was grown in standard CVD method.[41] To enhance the quality of graphene, 99.98% pure copper foils made of Aldrich was used. Before CVD deposition, the copper foils were polished by electrolysis of 85% H_3PO_4 for 17.5 min at 1.7 V. To avoid host atom doping into the copper during electrolysis, a counter electrode of copper was used. The polished copper was then put in to the CVD furnace for 60 min to preanneal at 1000 °C with 60 SCCM H_2 flow before growing graphene. Then 3.4 SCCM methane was allowed to flow for next 30 min keeping the previous condition same. A single layer graphene was deposited on both sides of the copper due to chemical reaction of H_2 and CH_4 at 1000 °C. To transfer the graphene on SiO_2 and PZT, PMMA on Cu/graphene was coated and floated it on $Fe_2(NO_3)_3$ solution to etch the Cu. When the copper was completely etched, the graphene/PMMA was transferred on DI water to wash out the remaining $Fe_2(NO_3)_3$ from it. Finally, it was collected on the top of SiO_2 and PZT substrates. To wash out the PMMA from SiO_2, it was immerged in the sample acetone at 80 °C for few minutes. Then it was dried. For PZT sample, PZT/graphene/PMMA composite was kept into a steady flow acetone vapor for 15–20 min; the sample was then washed by acetone and dried it. The quality of the graphene was investigated by performing the Raman spectroscopy with an excitation of 633 nm laser.

T1000 Cu mesh of Electron Microscopy Science was used as a mask to pattern the electrodes on the graphene/PZT and graphene/SiO_2 film which can produce 6 µm × 19 µm device with 6 µm channel length as shown in the inset of Figure 3a—c. After masking the active area, 5 nm of Ti and 100 nm Au were then deposited on it by thermal evaporator. Finally, the copper mask was taken out and GQD solution was spin-coated on the device. To improve the junction between GQD and graphene, the device was annealed for 5–10 min at 80 °C.

To get the optimum thickness of GQD layer, device with different thickness of QD layer was made by varying the spinning speed of the spin coater as shown in Figure S4 (Supporting Information). The optimum thickness of QD layer was achieved to show highest response is 46 nm, Figure S5 (Supporting Information), which is approximately equivalent to 6–7 layers of GQD.

Transfer characteristics of the device were measured using 4156C semiconductor parameter analyzer of Agilent. Dynamic response was carried out by Keithley 236 electrometer and 325 nm He—Cd UV laser. All the characterizations of the device were performed in ambient conditions.

Supporting Information

Supporting Information is available from the Wiley Online Library or from the author.

[1] K. S. Novoselov, A. K. Geim, S. V. Morozov, D. Jiang, Y. Zhang, S. V. Dubonos, I. V. Grigorieva, A. A. Firsov, *Science* **2004**, *306*, 666.

[2] Y. Zhang, Y.-W. Tan, H. L. Stormer, P. Kim, *Nature* **2005**, *438*, 201.

[3] A. K. Geim, *Science* **2009**, *324*, 1530.

www.MaterialsViews.com

ADVANCED
FUNCTIONAL
MATERIALS
www.afm-journal.de

FULL PAPER

[4] A. K. Geim, K. S. Novoselov, *Nat. Mater.* **2007**, *6*, 183.

[5] Y. Zhu, S. Murali, W. Cai, X. Li, J. W. Suk, J. R. Potts, R. S. Ruoff, *Adv. Mater.* **2010**, *22*, 3906.

[6] C. N. R. Rao, A. K. Sood, K. S. Subrahmanyam, A. Govindaraj, *Angew. Chem., Int. Ed.* **2009**, *48*, 7752.

[7] K. S. Novoselov, A. K. Geim, S. V. Morozov, D. Jiang, M. I. Katsnelson, I. V. Grigorieva, S. V. Dubonos, A. A. Firsov, *Nature* **2005**, *438*, 197.

[8] R. R. Nair, P. Blake, A. N. Grigorenko, K. S. Novoselov, T. J. Booth, T. Stauber, N. M. R. Peres, A. K. Geim, *Science* **2008**, *320*, 1308.

[9] M. Yankowitz, J. Xue, D. Cormode, J. D. Sanchez-Yamagishi, K. Watanabe, T. Taniguchi, P. Jarillo-Herrero, P. Jacquod, B. J. LeRoy, *Nat. Phys.* **2012**, *8*, 382.

[10] G. Konstantatos, M. Badioli, L. Gaudreau, J. Osmond, M. Bernechea, F. P. G. de Arquer, F. Gatti, F. H. L. Koppens, *Nat. Nanotechnol.* **2012**, *7*, 363.

[11] M.-L. Lu, C.-W. Lai, H.-J. Pan, C.-T. Chen, P.-T. Chou, Y.-F. Chen, *Nano Lett.* **2013**, *13*, 1920.

[12] S.-H. Cheng, T.-M. Weng, M.-L. Lu, W.-C. Tan, J.-Y. Chen, Y.-F. Chen, *Sci. Rep.* **2013**, *3*, 2694.

[13] B. M. Novak, *Adv. Mater.* **1993**, *5*, 422.

[14] Q. Li, N. Mahmood, J. Zhu, Y. Hou, S. Sun, *Nano Today* **2014**, *9*, 668.

[15] V. Gupta, N. Chaudhary, R. Srivastava, G. D. Sharma, R. Bhardwaj, S. Chand, *J. Am. Chem. Soc.* **2011**, *133*, 9960.

[16] Z. Zhang, J. Zhang, N. Chen, L. Qu, *Energy Environ. Sci.* **2012**, *5*, 8869.

[17] P. Roy, A. P. Periasamy, C. Chuang, Y.-R. Liou, Y.-F. Chen, J. Joly, C.-T. Liang, H.-T. Chang, *New J. Chem.* **2014**, *38*, 4946.

[18] Z. L. Wang, J. Song, *Science* **2006**, *312*, 242.

[19] F. Gattringer, M. Nader, M. Krommer, H. Irschik, *J. Vib. Control* **2003**, *9*, 965.

[20] X. Wang, J. Zhou, J. Song, J. Liu, N. Xu, Z. L. Wang, *Nano Lett.* **2006**, *6*, 2768.

[21] F. Bonaccorso, Z. Sun, T. Hasan, A. C. Ferrari, *Nat. Photonics* **2010**, *4*, 611.

[22] C.-Y. Hsieh, M.-L. Lu, J.-Y. Chen, Y.-T. Chen, Y.-F. Chen, W. Y. Shih, W.-H. Shih, *Nanotechnology* **2012**, *23*, 355201.

[23] C.-Y. Hsieh, Y.-T. Chen, W.-J. Tan, Y.-F. Chen, W. Y. Shih, W.-H. Shih, *Appl. Phys. Lett.* **2012**, *100*, 113507.

[24] W.-C. Tan, W.-H. Shih, Y. F. Chen, *Adv. Funct. Mater.* **2014**, *24*, 6818.

[25] Z. Sun, Z. Liu, J. Li, G.-A. Tai, S.-P. Lau, F. Yan, *Adv. Mater.* **2012**, *24*, 5878.

[26] V. Q. Dang, T. Q. Trung, D.-I. Kim, L. T. Duy, B.-U. Hwang, D.-W. Lee, B.-Y. Kim, L. D. Toan, N.-E. Lee, *Small* **2015**, *25*, 3054.

[27] C. O. Kim, S. W. Hwang, S. Kim, D. H. Shin, S. S. Kang, J. M. Kim, C. W. Jang, J. H. Kim, K. W. Lee, S.-H. Choi, E. Hwang, *Sci. Rep.* **2014**, *4*, 5603.

[28] Y. Lee, J. Kwon, E. Hwang, C. H. Ra, W. J. Yoo, J. H. Ahn, J. H. Park, J. H. Cho, *Adv. Mater.* **2015**, *27*, 41.

[29] F. Withers, T. H. Bointon, M. F. Craciun, S. Russo, *ACS Nano* **2013**, *7*, 5052.

[30] L. Tang, R. Ji, X. Cao, J. Lin, H. Jiang, X. Li, K. S. Teng, C. M. Luk, S. Zeng, J. Hao, S. P. Lau, *ACS Nano* **2012**, *6*, 5102.

[31] J. Peng, W. Gao, B. K. Gupta, Z. Liu, R. Romero-Aburto, L. Ge, L. Song, L. B. Alemany, X. Zhan, G. Gao, S. A. Vithayathil, B. A. Kaipparettu, A. A. Marti, T. Hayashi, J.-J. Zhu, P. M. Ajayan, *Nano Lett.* **2012**, *12*, 844.

[32] A. C. Ferrari, J. C. Meyer, V. Scardaci, C. Casiraghi, M. Lazzeri, F. Mauri, S. Piscanec, D. Jiang, K. S. Novoselov, S. Roth, A. K. Geim, *Phys. Rev. Lett.* **2006**, *97*, 87401.

[33] D. Graf, F. Molitor, K. Ensslin, C. Stampfer, A. Jungen, C. Hierold, L. Wirtz, *Nano Lett.* **2007**, *7*, 238.

[34] A. Reina, X. Jia, J. Ho, D. Nezich, H. Son, V. Bulovic, M. S. Dresselhaus, J. Kong, *Nano Lett.* **2009**, *9*, 30.

[35] Y. Shi, W. Fang, K. Zhang, W. Zhang, L.-J. Li, *Small* **2009**, *5*, 2005.

[36] H. Lee, Y. S. Kang, S.-J. Cho, B. Xiao, H. Morkoc, T. D. Kang, G. S. Lee, J. Li, S.-H. Wei, P. G. Snydar, J. T. Evans, *J. Appl. Phys.* **2005**, *98*, 094108.

[37] Y.-J. Yu, Y. Zhao, S. Ryu, L. E. Brus, K. S. Kim, P. Kim, *Nano. Lett* **2009**, *9*, 3430.

[38] M.-L. Lu, T.-M. Weng, J.-Y. Chen, Y.-F. Chen, *NPG Asia Mater.* **2012**, *4*, e26.

[39] Y. Li, Y. Hu, Y. Zhao, G. Shi, L. Deng, Y. Hou, L. Qu, *Adv. Mater.* **2011**, *23*, 776.

[40] B. Chitara, L. S. Panchakarla, S. B. Krupanidhi, C. N. R. Rao, *Adv. Mater.* **2011**, *23*, 5419.

[41] X. Li, W. Cai, J. An, S. Kim, J. Nah, D. Yang, R. Piner, A. Velamakanni, I. Jung, E. Tutuc, S. K. Banerjee, L. Colombo, R. S. Ruoff, *Science* **2009**, *324*, 1312.